Clustering and redshift-space distortions in interacting dark energy cosmologies

Federico Marulli^{1,2,3}, Marco Baldi^{4,5} and Lauro Moscardini^{1,2,3}

- ¹Dipartimento di Astronomia, Alma Mater Studiorum Università di Bologna, via Ranzani 1, I-40127 Bologna, Italy
- ²INAF-Osservatorio Astronomico di Bologna, Via Ranzani 1, 40127, Bologna, Italy
- ³INFN/National Institute for Nuclear Physics, Sezione di Bologna, viale Berti Pichat 6/2, I-40127 Bologna, Italy
- ⁴ Excellence Cluster Universe, Boltzmannstr. 2, D-85748 Garching, Germany
- ⁵ University Observatory, Ludwig-Maximillians University Munich, Scheinerstr. 1, D-81679 Munich, Germany

1 November 2021

ABSTRACT

We investigate the spatial properties of the large scale structure (LSS) of the Universe in the framework of coupled dark energy (cDE) cosmologies. Using the public halo catalogues from the CoDECS simulations - the largest set of N-body experiments to date for such cosmological scenarios – we estimate the clustering and bias functions of cold dark matter (CDM) haloes, both in real- and redshift-space. Moreover, we investigate the effects of the dark energy (DE) coupling on the geometric and dynamic redshift-space distortions, quantifying the difference with respect to the concordance Λ CDM model. At $z \sim 0$, the spatial properties of CDM haloes in cDE models appear very similar to the ACDM case, even if the cDE models are normalized at last scattering in order to be consistent with the latest Cosmic Microwave Background (CMB) data. At higher redshifts, we find that the DE coupling produces a significant scale-dependent suppression of the halo clustering and bias function. This effect, that strongly depends on the coupling strength, is not degenerate with σ_8 at scales $r \lesssim 5-10$ h^{-1} Mpc. Moreover, we find that the coupled DE strongly affects both the linear distortion parameter, β , and the pairwise peculiar velocity dispersion, σ_{12} . Although the models considered in this work are found to be all in agreement with presently available observational data, the next generation of galaxy surveys will be able to put strong constraints on the level of coupling between DE and CDM exploiting the shape of redshift-space clustering anisotropies.

Key words: cosmology: theory – cosmology: observations, dark matter, dark energy, galaxy clustering

1 INTRODUCTION

The concordance ACDM cosmological model has strongly improved its reputation over the last two decades thanks to the overall agreement between its predictions and the ever increasing wealth of available observational data (see e.g. Riess et al. 1998; Perlmutter et al. 1999; Percival et al. 2001; Spergel et al. 2003; Astier et al. 2006; Komatsu et al. 2009; Crocce et al. 2011; Carnero et al. 2011). However, some possible tensions between the predictions of the ACDM scenario and astrophysical observations at small scales have also been claimed, like the abundance of satellite galaxies in CDM haloes, the low baryon fraction in galaxy clusters and the 'cusp-core' problem for the halo density profiles (see e.g. Allen et al. 2004; LaRoque et al. 2006; Vikhlinin et al. 2006; Simon et al. 2003; Binney & Evans 2001; Newman et al. 2009). It is still unclear whether such discrepancies might be due to an incorrect description of the baryonic phenomena at work, or if they are directly connected to the underlying cosmological scenario. In any case, it is interesting to investigate how the standard ACDM model could be modified in order to better match the above-mentioned observations.

Furthermore, the fundamental nature of CDM particles and of the DE component - that together constitute more than 95% of the total energy of the Universe - is still unknown, which represents one of the central problems of modern cosmology. From an observational point of view, the existence of a stress-energy component with negative pressure, responsible for the accelerated expansion of the Universe, can be directly deduced from supernova measurements (see e.g. Riess et al. 1998; Perlmutter et al. 1999; Schmidt et al. 1998; Astier et al. 2006; Kowalski et al. 2008), or by jointly combining the CMB power spectrum and low redshift observations, like measurements of the Hubble constant, of the galaxy power spectrum and of cluster counts. More recently, by combining the CMB lensing deflection power spectrum from the Atacama Cosmology Telescope with temperature and polarization power spectra from the Wilkinson Microwave Anisotropy Probe, it has been possible to break the geometric degeneracy and constrain

the dark energy density using measurements of the CMB radiation alone (Sherwin et al. 2011).

Several theoretical efforts have been made in order to find a satisfactory explanation for the cosmic acceleration. Different DE models have been proposed in the literature, ranging from simple scenarios with a constant equation of state to models considering interactions between DE and other cosmic fluids, as e.g. CDM (see e.g. Wetterich 1995; Amendola 2000) or massive neutrinos (Amendola et al. 2008). Indeed, if the accelerated expansion is driven by a scalar field, there is no fundamental reason why DE and CDM should not interact with each other. Interestingly, it has been shown that such a direct coupling could help in alleviating some of the small-scale problems of the ACDM cosmology (see e.g. Baldi et al. 2010; Baldi & Pettorino 2011; Lee & Baldi 2011).

In the present paper, we investigate the spatial properties of LSS predicted by interacting DE cosmological models. In particular, this work is focused on the clustering and bias properties of CDM haloes and on their redshift-space clustering distortions (RSD) caused by the line-of-sight component of galaxy peculiar velocities. The latest galaxy surveys that have enabled measurements of RSD are the 2-degree Field Galaxy Redshift Survey (Peacock et al. 2001; Hawkins et al. 2003; Percival et al. 2004), the Sloan Digital Sky Survey (Tegmark et al. 2004; Zehavi et al. 2005; Tegmark et al. 2006; Okumura et al. 2008; Cabré & Gaztañaga 2009a,b) and the VIMOS-VLT Deep Survey (Guzzo et al. 2008).

RSD can be used to probe gravity theories, as they are directly related to the growth rate of LSS (Linder 2008). Moreover, they can also be used in several other contexts, e.g. to robustly constrain the value of the total mass of cosmological neutrinos (Marulli et al. 2011) or to investigate the dynamical properties of the warm-hot intergalactic medium (Ursino et al. 2011). Since the interaction between DE and CDM strongly affects the formation and evolution of LSS, a significant effect on RSD is also expected. To properly describe all the non-linear effects at work, we use a series of stateof-the-art N-body simulations for a wide range of different cDE scenarios - the CoDECS simulations (Baldi 2011c) - and discuss the impact that DE interactions can have on LSS with respect to the ACDM case. Both on-going and next generation galaxy surveys, such as VIPERS (Guzzo et al. 2011 in preparation), BigBOSS (Schlegel et al. 2009) and Euclid (Laureijs 2009; Refregier et al. 2010), will greatly improve the precision in RSD measurements over an even grater redshift range, up to z = 2, allowing for direct constraints on the underlying cosmological model and on the grav-

The structure of the paper is as follows. In section §2 we describe the cDE models analyzed in this work, while in section §3 we introduce the exploited set of N-body experiments used to simulate the LSS in these cosmological frameworks. In section §4 we analyze the CDM halo clustering and bias functions and the redshiftspace clustering distortions. Finally, in section §5 we draw our conclusions.

THE COUPLED DARK ENERGY MODELS

Interacting DE scenarios have been introduced as a possible alternative to the standard ACDM cosmology (Wetterich 1995; Amendola 2000) with the aim of addressing the fine-tuning problems that characterize the cosmological constant. These alternative cosmologies include models where a DE scalar field ϕ interacts with other cosmic fluids by exchanging energy-momentum during the evolution of the universe. Several possible forms of DE interaction have been proposed in the literature, including e.g. models of coupling to the CDM fluid (as e.g. Amendola 2000, 2004; Koyama et al. 2009; Honorez et al. 2010; Baldi 2011d) or to massive neutrinos (Amendola et al. 2008). In the present work, we will focus on the former class, considering a DE-CDM interaction defined by the following set of background dynamic equations:

$$\ddot{\phi} + 3H\dot{\phi} + \frac{dV}{d\phi} = \sqrt{\frac{2}{3}}\eta_c(\phi)\frac{\rho_c}{M_{\rm Pl}}, \qquad (1)$$

$$\dot{\rho}_c + 3H\rho_c = -\sqrt{\frac{2}{3}}\eta_c(\phi)\frac{\rho_c\dot{\phi}}{M_{\rm Pl}}, \qquad (2)$$

$$\dot{\rho}_b + 3H\rho_b = 0, \tag{3}$$

$$\dot{\rho}_r + 4H\rho_r = 0, \tag{4}$$

$$\dot{\rho}_{b} + 3H\rho_{b} = 0, \qquad (3)$$

$$\dot{\rho}_{r} + 4H\rho_{r} = 0, \qquad (4)$$

$$3H^{2} = \frac{1}{M_{\text{Pl}}^{2}} \left(\rho_{r} + \rho_{c} + \rho_{b} + \rho_{\phi} \right), \qquad (5)$$

where an overdot represents a derivative with respect to the cosmic time t, $H \equiv \dot{a}/a$ is the Hubble function, $V(\phi)$ is the scalar field selfinteraction potential, $M_{\rm Pl} \equiv 1/\sqrt{8\pi G}$ is the reduced Planck Mass, and the subscripts b, c, r indicate baryons, CDM, and radiation, respectively. The strength of the interaction between the DE scalar field and CDM particles is defined by the coupling function $\eta_c(\phi)$, while the shape of the potential $V(\phi)$ dictates the dynamical evolution of the DE field that in turn determines a time evolution of the CDM particle mass:

$$\frac{d\ln M_c}{dt} = -\sqrt{\frac{2}{3}}\eta_c(\phi)\dot{\phi},\tag{6}$$

as one can obtain from Eq. (2).

In this work, we will consider the set of coupled DE scenarios defined in Baldi (2011c), which includes two possible choices for the coupling function – namely a constant coupling $\eta_c = \eta_0$ and an exponential coupling $\eta_c(\phi) = \eta_0 \exp[\eta_1 \phi]$ and two possible forms of the scalar potential, namely an exponential potential (Lucchin & Matarrese 1985; Wetterich 1988):

$$V(\phi) = Ae^{-\alpha\phi} \tag{7}$$

and a SUGRA potential (Brax & Martin 1999):

$$V(\phi) = A\phi^{-\alpha}e^{\phi^2/2}, \tag{8}$$

where for simplicity the field ϕ has been expressed in units of the reduced Planck mass in Eqs. (7,8). The parameters of the models investigated in the present work are summarized in Table 1.

At the linear perturbations level, the time evolution of density fluctuations in the coupled CDM fluid and in the uncoupled baryonic component ($\delta_{c,b} \equiv \delta \rho_{c,b}/\rho_{c,b}$, respectively) obeys the following system of equations:

$$\ddot{\delta}_{c} = -2H \left[1 - \eta_{c} \frac{\dot{\phi}}{H\sqrt{6}} \right] \dot{\delta}_{c} + 4\pi G \left[\rho_{b} \delta_{b} + \rho_{c} \delta_{c} \Gamma_{c} \right], \tag{9}$$

$$\ddot{\delta}_b = -2H\dot{\delta}_b + 4\pi G[\rho_b \delta_b + \rho_c \delta_c], \qquad (10)$$

where for simplicity the field dependence of the coupling function $\eta_c(\phi)$ has been omitted. In Eq. (9), the factor $\Gamma_c \equiv 1 + 4\eta_c^2(\phi)/3$ encodes the effect of the additional fifth-force mediated by the DE scalar field ϕ for CDM perturbations. Additionally, the second term in the first square bracket at the right-hand-side of Eq. (9) represents an extra-friction term on CDM fluctuations arising as a consequence of momentum conservation (see e.g. Amendola 2004; Pettorino & Baccigalupi 2008; Baldi et al. 2010; Baldi 2011a, for

0.806

-0.901

Model	Potential	α	η_0	η_1	$w_{\phi}(z=0)$	$\sigma_8(z=0)$
ΛCDM	$V(\phi) = A$	_	_	-	-1.0	0.809
EXP001	$V(\phi) = Ae^{-\alpha\phi}$	0.08	0.05	0	-0.997	0.825
EXP002	$V(\phi) = Ae^{-\alpha\phi}$	0.08	0.1	0	-0.995	0.875
EXP003	$V(\phi) = Ae^{-\alpha\phi}$	0.08	0.15	0	-0.992	0.967
EXP008e3	$V(\phi) = Ae^{-\alpha\phi}$	0.08	0.4	3	-0.982	0.895

Table 1. The list of cosmological models considered in the CoDECS project and their specific parameters.

 $V(\phi) = A\phi^{-\alpha}e^{\phi^2/2}$

a derivation of Eqs. (1-5,9,10) and for a detailed discussion of the extra-friction and fifth-force corrections to the evolution of linear perturbations).

SUGRA003

The background and linear perturbations evolution of all the cosmologies considered in this work have been discussed in full detail in Baldi (2011b) and Baldi (2011c), to which we refer the interested reader for a more thorough description of the models. In particular, the EXP008e3 model - based on an exponential potential and on an exponential coupling function - features a steep growth of the interaction strength at low redshifts and has been shown to significantly enhance the pairwise infall velocity of colliding galaxy clusters similar to the "Bullet Cluster" (Lee & Baldi 2011). On the other hand, the SUGRA003 model based on a SUGRA potential and on a negative constant coupling is an example of the recently proposed "Bouncing" cDE scenario (Baldi 2011b), which is characterized by an inversion of the scalar field direction of motion at relatively recent epochs ($z_{\rm inv} \approx 6.8$ for the specific model under investigation), giving rise to a "bounce" of the DE equation of state parameter w_{ϕ} on the cosmological constant barrier $w_{\phi} = -1$. As a consequence of such inversion, the quantity $\eta_c \dot{\phi}$ that appears both in Eqs. (6) and (9) changes sign in correspondence to the bounce such that the CDM particle mass decreases before the bounce and increases again afterwards, while the extra-friction term changes from a drag to a proper friction at z_{inv} . Such peculiar dynamical behaviour has been shown to provide a possible explanation (Baldi 2011b) to the recent detections of massive clusters of galaxies at high redshifts (Jee et al. 2009; Rosati et al. 2009), although the statistical significance of such detections as a challenge to the standard ACDM scenario is presently not yet conclusive (see e.g. Mortonson et al. 2011; Waizmann et al. 2011).

3 THE N-BODY SIMULATIONS

For our investigation we rely on the public halo catalogues of the CoDECS simulations (Baldi 2011c), the largest N-body simulations for cDE cosmologies to date, that include all the models described in Table 1. In particular, we make use of the L-CoDECS suite which consists of large scale, collisionless N-body runs following the evolution of 1024^3 CDM particles and 1024^3 baryonic particles in a cosmological box of 1 comoving Gpc/h on a side. The simulations have been carried out with the modified version by Baldi et al. (2010) of the widely used parallel Tree-PM N-body code GADGET (Springel 2005), and have a mass resolution of $m_c(z=0)=5.84\times10^{10}~\mathrm{M}_\odot/h$ and $m_b=1.17\times10^{10}~\mathrm{M}_\odot/h$ for CDM and baryons, respectively, and a force resolution of $\epsilon_g=20~\mathrm{kpc}/h$.

The initial conditions for all the different cosmologies were generated by perturbing a homogeneous "glass" distribution (White 1994; Baugh et al. 1995) based on the same linear power

spectrum at $z_{\rm CMB}$, and then rescaling the resulting displacements to the starting redshift of the simulations, $z_i = 99$, with the specific growth factor $D_+(z)$ of each model computed by numerically solving Eqs. (9,10). This procedure ensures that all the models are consistent with the same normalization of density perturbations at the last scattering surface, which has been assumed to correspond to the "WMAP7 Only Maximum Likelihood" constraints of Komatsu et al. (2011). The cosmological parameters at z=0 assumed for all the models included in the CoDECS project are $H_0=70.3\,{\rm km\,s^{-1}\,Mpc^{-1}}$, $\Omega_{\rm CDM}=0.226$, $\Omega_{\rm DE}=0.729$, $\sigma_8=0.809$, $\Omega_b=0.0451$ and $n_s=0.966$.

The halo catalogues have been obtained by identifying groups of particles by means of a Friends-of-Friends (FoF, Davis et al. 1985) algorithm with linking length $\lambda = 0.2 \times \bar{d}$, where \bar{d} is the mean interparticle separation. The FoF algorithm was run over the CDM particles as primary tracers of the matter distribution, and then baryonic particles have been attached to the FoF group of their closest CDM neighbour. In order to identify CDM substructures we have used the SUBFIND algorithm described in Springel et al. (2001). All the results presented in this paper have been obtained using mass-selected sub-halo catalogues, composed by the gravitationally bound substructures that SUBFIND identifies in each FoF halo. For all the simulations, we have restricted our analysis in the mass range $M_{\rm min} < M < M_{\rm max}$, where $M_{\rm min} = 2.5 \cdot 10^{12} M_{\odot}/h$ and $M_{\rm max} = 3.6 \cdot 10^{15}, 1.1 \cdot 10^{15}, 4.9 \cdot 10^{14}, 2.6 \cdot 10^{14}, 1.8 \cdot 10^{14} M_{\odot}/h$ at z = 0, 0.55, 1, 1.6, 2, respectively. For the analysis presented in this paper, we have used one realisation of each model. To investigate how reliable our results are, we have divided each simulation box in 27 independent sub-boxes and estimated the uncertainties in our predictions from the scatter between them. At the scales considered, we found a very good agreement between the errors estimated in this way and the theoretical ones, both for the correlation function and for the bias.

4 LSS IN CDE MODELS

In this section we show how the halo clustering, the bias function and the redshift-space distortion parameters β and σ_{12} get modified, with respect to the standard Λ CDM case, when CDM and DE can interact with each other.

4.1 The DM halo clustering in real space

In cDE scenarios the formation and evolution of cosmic structures can differ significantly with respect to the Λ CDM case. To analyze the spatial properties of LSS as a function of the DE coupling, we measure the CDM halo two-point correlation function, $\xi(r)$, de-



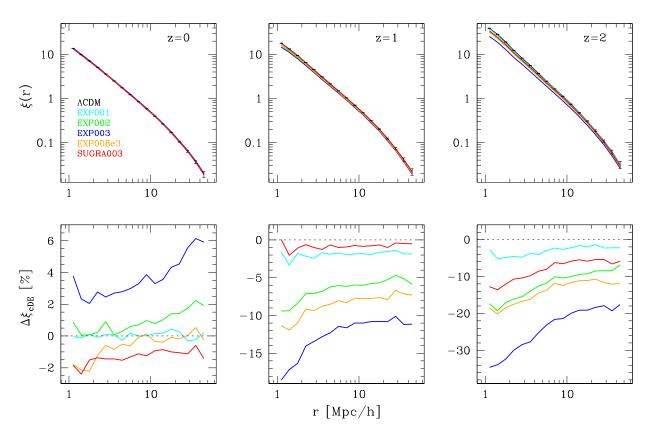


Figure 1. Upper panels: real-space two-point correlation function of CDM haloes for all the models of the CoDECS project. The black error bars represent the statistical noise as prescribed by Mo et al. (1992). Lower panels: percentage difference between cDE and Λ CDM predictions, $\Delta \xi_{cDE} = 100 \cdot (\xi_{cDE} - \xi_{\Lambda CDM})/\xi_{\Lambda CDM}$. At z=0, the spatial properties of CDM haloes in cDE models are very similar to the Λ CDM case. However, at higher redshifts the DE coupling produces a significant scale-dependent suppression in the halo clustering.

fined as:

$$dP = n^{2}[1 + \xi(r)]dV_{1}dV_{2}, \tag{11}$$

where dP is the probability of finding a halo pair with one of them in the volume dV_1 and the other in the volume dV_2 , separated by a comoving distance r. To measure the function $\xi(r)$, we use the standard Landy & Szalay (1993) estimator:

$$\hat{\xi}(r) = \frac{HH(r) - 2RH(r) + RR(r)}{RR(r)},\tag{12}$$

where HH(r), HR(r) and RR(r) are the fraction of halo-halo, halo-random and random-random pairs, with spatial separation in the range [r-dr/2,r+dr/2]. The random samples are three times larger than the halo ones. A computationally efficient linked-list algorithm has been used to count the number of pairs in the halo and random catalogues.

Fig. 1 shows the real-space two-point correlation function of CDM haloes for all the models of the CoDECS project. The black error bars represent the statistical noise as prescribed by Mo et al. (1992). The lower panels show the percentage difference between cDE and Λ CDM predictions, $\Delta\xi_{\rm cDE}=100\cdot(\xi_{\rm cDE}-\xi_{\Lambda{\rm CDM}})/\xi_{\Lambda{\rm CDM}}$. The z=0 spatial properties of CDM haloes in cDE models are very similar to the $\Lambda{\rm CDM}$ case. The EXP003 model shows the largest deviations that are in any case quite small, between $\sim 2\%$ and $\sim 6\%$ for comoving separation $< 50~h^{-1}{\rm Mpc}$. The situation is different at higher redshifts, where the DE coupling

produces a significant scale-dependent suppression in the halo clustering. This effect strongly depends on the coupling strength and on the redshift. At small scales, the deviations with respect to the ACDM predictions rise to $\sim 20\%$ at z=1 and $\sim 35\%$ at z=2 for the extreme EXP003 model. The EXP008e3 and SUGRA003 models predict a different redshift evolution in the clustering function with respect to the models with a constant coupling. Therefore, measuring the redshift evolution of $\xi(r)$ can help to disentangle different interacting DE cosmologies.

4.2 The CDM halo biasing function

The clustering suppression predicted by cDE models in massselected halo samples can be better understood by looking at the large-scale halo bias. Fig. 2 shows the mean *apparent* effective bias of CDM haloes defined as follows:

$$\langle b(z) \rangle = \langle \sqrt{\frac{\xi_{\text{halo,cDE}}}{\xi_{\text{DM,ACDM}(\sigma_8)}}} \rangle,$$
 (13)

where $\xi_{halo,cDE}$ is the cDE halo clustering and $\xi_{DM,ACDM(\sigma_8)}$ is the ΛCDM DM clustering normalized to the σ_8 values of the CoDECS models. $\xi_{DM,\Lambda CDM(\sigma_8)}$ has been obtained by Fourier transforming the non-linear power spectrum extracted from CAMB (Lewis & Bridle 2002), which exploits the HALOFIT routine (Smith et al. 2003). The bias is averaged in the range $10h^{-1}\,\mathrm{Mpc}$ <

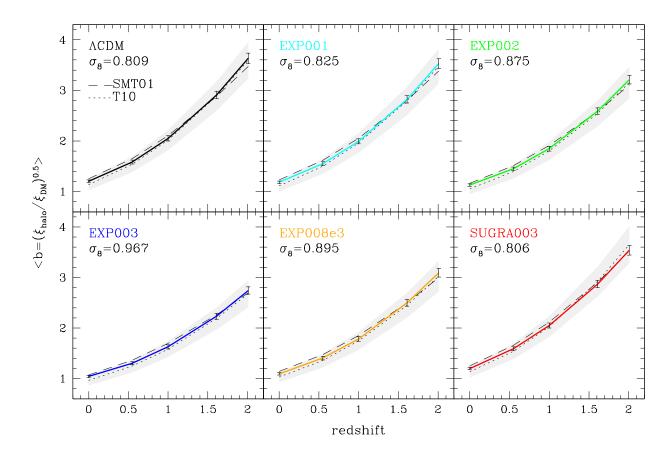


Figure 2. Mean apparent effective bias of CDM haloes, $< b> = < (\xi_{halo,cDE}/\xi_{DM,\Lambda CDM}(\sigma_8))^{0.5} >$, averaged in the range $10h^{-1}$ Mpc $< r < 50h^{-1}$ Mpc . Dashed and dotted black lines show the theoretical Λ CDM effective bias computed according to the relations of Sheth et al. (2001) and Tinker et al. (2010), respectively, normalized to the σ_8 values of the CoDECS models. The error bars represent the propagated statistical noise as prescribed by Mo et al. (1992), while the grey shaded areas show a 10% error. The effect of DE coupling on the CDM halo large scale bias appears totally degenerate with σ_8 for all the cosmological models considered.

 $r < 50h^{-1}\,\mathrm{Mpc}$. The error bars represent the propagated statistical noise as prescribed by Mo et al. (1992). By definition, < b(z) > represents the apparent bias that would be derived in a cDE universe if a $\Lambda\mathrm{CDM}$ model was erroneously assumed to predict the DM clustering.

Dashed and dotted black lines in Fig. 2 show the theoretical Λ CDM effective bias of Sheth et al. (2001) and Tinker et al. (2010), respectively, normalized to the values of σ_8 of the CoDECS models and weighted with the halo mass function, n(M,z):

$$b_{\text{eff}}(z) = \frac{\int_{M_{\text{min}}}^{M_{\text{max}}} n(M, z) b(M, z) dM}{\int_{M_{\text{min}}}^{M_{\text{max}}} n(M, z) dM},$$
(14)

where $M_{\rm min}$ and $M_{\rm max}$ have been defined in section §3. The grey shaded bands show a 10% error, that approximately represents the uncertainty in the theoretical bias predictions presented in the literature.

The effect of DE coupling on the CDM halo large-scale bias appears totally degenerate with σ_8 for all the cosmological models considered (see also Clemson et al. 2011, for a general discussion of degeneracies in cDE models). As already seen in Fig. 1, the halo clustering properties at small scales can help in removing this degeneracy. This can be better appreciated in Fig. 3 that shows CDM halo bias as a function of scale. The lower panels show

the percentage difference between cDE and Λ CDM predictions, $\Delta b_{\rm cDE} = 100 \cdot (b_{\rm cDE} - b_{\Lambda {\rm CDM}})/b_{\Lambda {\rm CDM}}$. Dashed and dotted lines refer to the theoretical Λ CDM predictions of Sheth et al. (2001) and Tinker et al. (2010), respectively, normalized to the values of σ_8 of the CoDECS models. It is clear that the scale-dependent suppression of the halo bias at small separations, due to the DE coupling, breaks the σ_8 degeneracy. Indeed, at scales $r \lesssim 5-10~h^{-1}{\rm Mpc}$, both the models with a constant coupling and the EXP008e3 one are not well reproduced by a standard Λ CDM model after having rescaled the matter power spectrum to the z=0 normalization of the cDE model. The SUGRA003 appears in better agreement with the Λ CDM predictions at $z \lesssim 1$, while at $z \gtrsim 2$ the halo bias of this model is not degenerate with σ_8 at all scales, although the effect is quite small ($\sim 3\%$ at z=2).

4.3 Redshift-space clustering distortions

4.3.1 Clustering shape in redshift-space

The redshift of a galaxy does not correspond to a unique distance from the observer, as the line-of-sight component of a galaxy's peculiar velocity creates an additional Doppler shift. When the distances are computed without correcting for this peculiar velocity

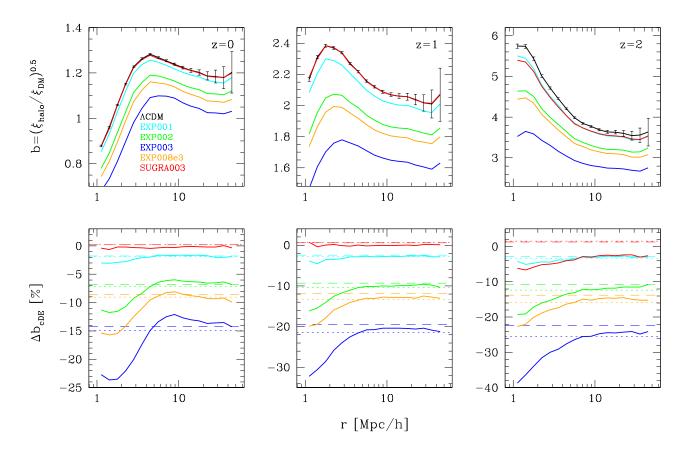


Figure 3. Upper panels: apparent effective bias of CDM halo as a function of scale, at three different redshifts z=0,1,2 from left to right. The error bars represent the statistical noise (Mo et al. 1992). Lower panels: percentage difference between cDE and Λ CDM predictions, $\Delta b_{\rm cDE}=100\cdot(b_{\rm cDE}-b_{\Lambda{\rm CDM}})/b_{\Lambda{\rm CDM}}$. Dashed and dotted lines show the theoretical Λ CDM predictions computed according to the relations of Sheth et al. (2001) and Tinker et al. (2010), respectively, normalized to the z=0 values of σ_8 of the CoDECS models. The scale-dependent suppression of the halo bias at small separations ($r\lesssim 5-10~h^{-1}{\rm Mpc}$) due to the DE coupling breaks the σ_8 degeneracy.

contribution, we say to be in *redshift-space* and we refer to the redshift-space spatial coordinates using the vector \vec{s} (while \vec{r} indicates real-space coordinates). A redshift-space galaxy map is distorted with respect to the *real* one. RSD provide crucial constraints on the build-up of LSS. On small scales ($\lesssim 1~h^{-1}{\rm Mpc}$) the distortion is mainly caused by the random orbital motions of galaxies moving inside virialised structures, i.e. the well-known *fingers of God* effect (Jackson 1972). On larger distance scales, the coherent bulk motion of virialising structures leads to an apparent excess in the clustering strength perpendicularly to the line-of-sight.

Since both comoving coordinates and peculiar velocities are known in an N-body simulation, we can investigate the spatial properties of LSS both in real- and redshift-space. To obtain redshift-space halo maps, we locate a virtual observer at z=0 and put each simulation box at a comoving distance corresponding to its output redshifts. The redshift-space distance of each CDM halo is obtained through the following equation:

$$s_{\parallel} = \int_0^{z_{\text{obs}}} \frac{cdz'_{\text{obs}}}{H(z'_{\text{obs}})},\tag{15}$$

where $H(z'_{\text{obs}})$ is the Hubble rate, c is the speed of light and the observed redshift, z_{obs} , is given by:

$$z_{\text{obs}} = z_{\text{c}} + \frac{v_{\parallel}}{c} (1 + z_{\text{c}}).$$
 (16)

Here z_c is the *cosmological* redshift, due to the Hubble flow, while the second term of Eq. (16) is caused by galaxy peculiar velocities (v_{\parallel}) is the component of the peculiar velocity parallel to the line-of-sight).

Whether the cosmological parameters assumed in Eq. (15) are not the true ones, or the Universe is not described by the Λ CDM equations, like in the cDE scenarios, a *geometric* kind of distortion is added to the *dynamic* distortion caused by peculiar velocities (Alcock & Paczynski 1979). However, as we will see in Sec. 4.3.2, geometric distortions in cDE models are rather small relative to the dynamical ones and can therefore be neglected.

Such a simple method to derive redshift-space coordinates is not as accurate as a full past light-cone reconstruction (see e.g. Marulli et al. 2009), since it neglects the redshift evolution of halo properties inside each snapshot box. However, this method is accurate enough for the purpose of the present work. In a companion paper we aim to estimate the expected observational uncertainties in constraining cDE model parameters with next generation galaxy surveys, and for that specific goal realistic mock galaxy catalogues will be constructed.

To extract cosmological constraints from RSD it is convenient to decompose the distances into the two components perpendicular and parallel to the line-of-sight, $\vec{r}=(r_\perp,r_\parallel)$. When measured in real-space, the contour lines of $\xi(r_\perp,r_\parallel)$ are circles, as the popula-

tion of haloes/galaxies is isotropic when averaged on large scales. Instead, the redshift-space correlation function is distorted: at small scales, the *fingers of God* effect changes the shape of correlation in the direction parallel to the line-of-sight, while at large scales the bulk motion squashes the correlation perpendicularly to the line-of-sight. These effects can be clearly seen in Fig. 4, where the contour lines of the two-point redshift-space correlation function of CDM haloes are shown. We also plot in the same panels the undistorted real-space correlation function (dotted grey lines) for comparison.

4.3.2 Modelling the dynamical redshift-space distortions

Assuming the plane-parallel approximation, the linear power spectrum of the matter density fluctuations, P(k), can be parameterized in redshift-space as follows:

$$P(k) = (1 + \beta \mu^2)^2 P_{\text{lin}}(k), \tag{17}$$

where $P_{lin}(k)$ is the linear power spectrum in real-space, μ is the cosine of the angle between \vec{k} and the line-of-sight and β is the linear distortion parameter. Fourier transforming equation (17) gives

$$\xi(s,\mu) = \xi_0(s)P_0(\mu) + \xi_2(s)P_2(\mu) + \xi_4(s)P_4(\mu), \tag{18}$$

where the functions P_l are the Legendre polynomials (Hamilton 1992), while the multipoles, $\xi_n(s)$, can be written as follows

$$\xi_0(s) = \left(1 + \frac{2\beta}{3} + \frac{\beta^2}{5}\right)\xi(r),\tag{19}$$

$$\xi_2(s) = \left(\frac{4\beta}{3} + \frac{4\beta^2}{7}\right) [\xi(r) - \overline{\xi}(r)],$$
 (20)

$$\xi_4(s) = \frac{8\beta^2}{35} \left[\xi(r) + \frac{5}{2} \overline{\xi}(r) - \frac{7}{2} \overline{\overline{\xi}}(r) \right]. \tag{21}$$

Here $\xi(r)$ is the real-space correlation function and the *barred* correlation functions are defined as

$$\overline{\xi}(r) = \frac{3}{r^3} \int_0^r dr' \xi(r') r'^2, \tag{22}$$

$$\overline{\overline{\xi}}(r) = \frac{5}{r^5} \int_0^r dr' \xi(r') r'^4.$$
 (23)

To include in the model also the small non-linear scales, we convolve it with the distribution function of random pairwise velocities, f(v) (but see e.g. Scoccimarro 2004; Matsubara 2004):

$$\xi(s_{\perp}, s_{\parallel}) = \int_{-\infty}^{\infty} dv f(v) \xi(s_{\perp}, s_{\parallel} - v/H(z)/a(z)). \tag{24}$$

In this work, we adopt for f(v) the form

$$f_{\text{exp}}(v) = \frac{1}{\sigma_{12}\sqrt{2}} \exp\left(-\frac{\sqrt{2}|v|}{\sigma_{12}}\right),$$
 (25)

where σ_{12} is the dispersion in the pairwise peculiar velocities.

To summarize, the model for the distorted correlation function in redshift-space (Eq. (24)) depends on the correlation function in real space, $\xi(r)$, and on two free parameters: the linear distortion parameter, β , and the pairwise peculiar velocities dispersion, σ_{12} . It can be demonstrated that β is well parameterized by the following equation:

$$\beta = \frac{f(\Omega_m)}{h} \simeq \frac{\Omega_m(z)^{\gamma}}{h},\tag{26}$$

where $f(\Omega_m) = d \ln D / d \ln a$ is the velocity growth rate, D is the

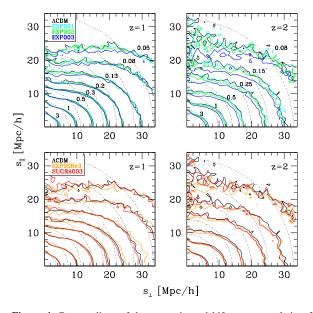


Figure 4. Contour lines of the two-point redshift-space correlation function of CDM haloes, $\xi(s_\perp,s_\parallel)$. The iso-curve plotted are $\xi(s_\perp,s_\parallel) = \{0.05,0.08,0.13,0.2,0.3,0.5,1,3\}$ and $\{0.08,0.15,0.25,0.5,1,3\}$ in the left and right panels, respectively. Dotted grey lines show the undistorted correlation function in real-space.

linear density growth factor, b is the linear CDM halo bias, and $\Omega_m(z)$ is the matter density. The so-called gravitational growth index, γ , directly depends on the gravity theory, being $\gamma \sim 0.545$ for GR gravity. As a consequence, observational constraints on the parameter β that can be obtained modelling the redshift-space correlation function $\xi(s_\perp,s_\parallel)$ directly translate to constraints on the gravity theory.

Fig. 5 shows the ratio between redshift- and real-space correlation functions of the CDM haloes in all the CoDECS simulations. The error bars represent the statistical noise (Mo et al. 1992). The black lines show the theoretical Λ CDM prediction given by the large-scale limit of Eq. (18):

$$\frac{\xi(s)}{\xi(r)} = 1 + \frac{2\beta}{3} + \frac{\beta^2}{5},\tag{27}$$

where $\beta = \frac{\Omega_m(z)^{0.545}}{b_{\rm eff}}$, and the effective bias $b_{\rm eff}$ is given by Eq. (14). Dashed and dotted black lines refer to the theoretical $\Lambda {\rm CDM}$ predictions obtained using the effective bias of Sheth et al. (2001) and Tinker et al. (2010), respectively, normalized to the values of σ_8 of the CoDECS models. The grey shaded area represents the propagated 10% theoretical bias error.

As expected, the measured and model ratios $\xi(s)/\xi(r)$ agree quite well in the Λ CDM model. The cosmic evolution of LSS in cDE models has the effect of significantly suppressing this ratio. However, as for the large-scale clustering and biasing function, RSD appears to be strongly degenerate with σ_8 at the scales and redshifts considered. Indeed, the mean ratio $\xi(s)/\xi(r)$ of CDM haloes in the cDE simulation can be reproduced quite well by the expected Λ CDM prediction rescaled at the σ_8 value of the cDE model. Only the SUGRA003 model appears not totally degenerate with σ_8 at z=0.5, but the effect is quite small.

To extract the cosmological information from RSD both at small and large scales, we use Eq. (24) to model the redshift-space correlation function $\xi(s_{\perp}, s_{\parallel})$, where the real-space $\xi(r)$ has been

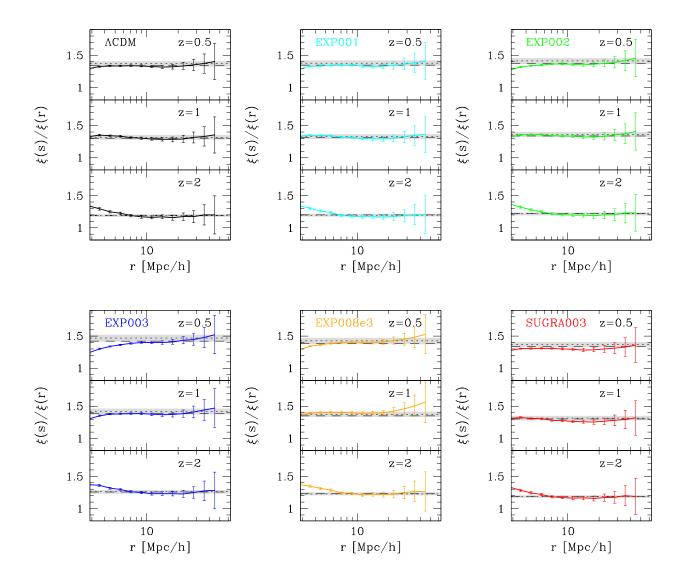


Figure 5. Ratio between redshift- and real-space correlation function of the CDM haloes. Dashed and dotted black lines show the theoretical Λ CDM predictions (Eq. (27)) using the effective bias functions computed according to the relations of Sheth et al. (2001) and Tinker et al. (2010), respectively, normalized to the values of σ_8 of the CoDECS models. The error bars represent the statistical noise (Mo et al. 1992). The DE coupling strongly affects the redshift-space clustering distortions. However such effect is strongly degenerate with σ_8 for the redshift considered. Only the SUGRA003 model appears not totally degenerate with σ_8 at z=0.5, but the effect is small.

measured using directly the comoving CDM halo model coordinates. The best-fit parameters, β and σ_{12} , obtained with a standard χ^2 minimization procedure are shown in the upper panels of Fig. 6, as a function of redshift. The errors on the best-fit parameter predictions have been estimated dividing the simulation box in 27 subboxes, measuring β and σ_{12} in each of them and rescaling their scatter by the square root of the total volume of the simulation box (see e.g. Marulli et al. 2011). The strong effect of cDE on both these parameters can be appreciated in the lower panels that show the percentage difference between cDE and Λ CDM predictions. Both in the models with a constant coupling and in the EXP008e3 one, β and σ_{12} are higher with respect to the Λ CDM case. This effect depends significantly on the coupling strenght and for the most extreme models considered raises to the level of \sim 20% for β and \sim 40% for σ_{12} . Viceversa, the SUGRA003 model predicts a sup-

pression of \sim 10% both in β and in σ_{12} at $z \sim 0.5-1$, while at higher redshifts the differences with respect to the Λ CDM model decrease.

This result suggests that using an independent constraint on σ_8 , that for instance can be obtained from the clustering and bias function at small scales (see Sec. 4.1 and 4.2), the next generation of galaxy surveys will be able to put strong constraints on the coupling between DE and CDM exploiting the shape of redshift-space clustering anisotropies.

4.3.3 Geometric distortions

In cDE scenarios, the relation between redshift and comoving distance is different from the one in the Λ CDM case. This means that if the Λ CDM equations are used to obtain galaxy maps from red-

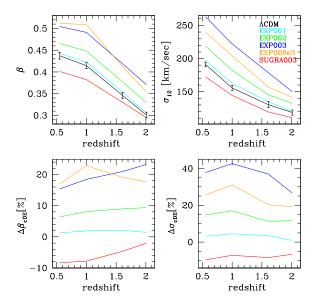


Figure 6. *Upper panels*: Best-fit parameters $\beta(z)$ (left panel) and $\sigma_{12}(z)$ (right panel) measured in all the CoDECS simulations. The error bars shown olny for ΛCDM represent the scatter in the measured β and σ_{12} obtained by dividing the simulation box in 27 sub-boxes, and rescaled by the square root of the total volume of the simulation box (see e.g. Marulli et al. 2011). *Lower panels*: percentage difference between cDE and ΛCDM predictions, $\Delta \beta_{cDE} = 100 \cdot (\beta_{cDE} - \beta_{\Lambda CDM})/\beta_{\Lambda CDM}$ (left panel), $\Delta \sigma_{cDE} = 100 \cdot (\sigma_{12,cDE} - \sigma_{12,\Lambda CDM})/\sigma_{12,\Lambda CDM}$ (right panel).

shift measurements in a Universe where DE and CDM interact, the correlation function appears distorted. To investigate the effect of such geometric distortions, also called Alcock-Paczynski distortions (Alcock & Paczynski 1979), we have repeated all the measurements described in the previous sections assuming the ΛCDM Hubble parameter H(z) in Eq. (15) to measure redshift-space distances also in the cDE simulations. Fig. 7 shows the percentage error on the best-fit parameters introduced in this way. In the three models with a constant coupling (EXP001, EXP002 and EXP003) these distortions slightly increase as a function of redshift, but only up to the level of $\sim 1\%$ for β and $\sim 2\%$ for σ_{12} at z=2, for the extreme EXP003 model. So, as expected, these distortions are quite small compared to the dynamical ones. Also in the EXP008e3 models the geometric distortions appear clearly negligible with respect to the dynamical distortions. Only the SUGRA003 model shows large geometric distortions, at a level of $\sim 5\%$ for β and $\sim 10\%$ for σ_{12} , comparable to the level of dynamical distortions. This suggests that geometric and dynamic distortions on the redshift-space clustering of galaxies might be strongly degenerate for the "Bouncing" cDE scenario, and independent measurements as e.g. the redshift evolution of the halo mass function should be used to break the degeneracy.

5 CONCLUSIONS

In the present paper we have investigated the impact of a possible interaction between DE and CDM on the clustering and redshift-space distortions of CDM haloes, also in view of the large wealth of high-quality data expected from the next generation of large galaxy surveys.

In cDE scenarios, in fact, the formation and evolution of LSS

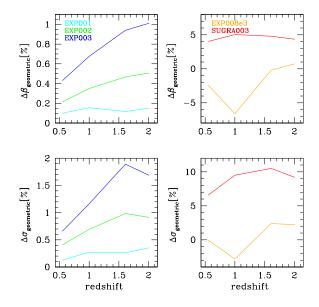


Figure 7. Percentage errors on the best-fit parameters $\beta(z)$ (left panel) and $\sigma_{12}(z)$ (right panel) introduced if Eq. (15) is used to measure redshift-space distances also in the cDE simulations.

can be significantly different with respect to the Λ CDM case. The interaction induces a time evolution of the mass of CDM particles as well as a modification of the growth of structures determined by the combined effect of a long-range fifth-force mediated by the DE scalar degree of freedom and of an extra-friction arising as a consequence of momentum conservation. The combination of these effects can significantly alter the evolution of linear and nonlinear density perturbations as compared to the standard Λ CDM scenario, and provide a direct way to test this class of cosmological models. In particular, the clustering properties of CDM haloes from linear to highly nonlinear scales might show specific signatures allowing to distinguish a cDE universe from Λ CDM.

In order to investigate the spatial properties of LSS in these cosmological scenarios it is therefore necessary to rely on a fully nonlinear treatment of structure formation in the context of cDE models. To this end, we made use of the public halo catalogues extracted from the largest set of N-body experiments to date for such cosmologies, the CoDECS simulations. From such catalogues, we measured the clustering and bias properties of CDM haloes both in real- and redshift-space, as a function of the DE coupling and redshift. Moreover, we investigated the effects of the DE coupling on the geometric and dynamic redshift-space distortions, quantifying the difference with respect to the concordance Λ CDM model. We compared numerical predictions with theoretical expectations finding a good agreement in Λ CDM, as expected, and a strong degeneracy between the DE coupling and the matter power spectrum normalization, σ_8 .

In particular, at $z\sim 0$ the spatial properties of CDM haloes in cDE models appear very similar to the Λ CDM case, even if the CoDECS simulations are normalized to be consistent with the latest CMB data at last scattering. At higher redshifts instead, we find that the DE coupling produces a significant scale-dependent suppression in the halo clustering and bias function. Furthermore, the DE coupling strongly affects the redshift-space clustering distortions. We quantified this effect by modelling RSD in terms of the redshift-space correlation function and the distribution function of

random pairwise velocities and deriving the linear distortion parameter, $\beta,$ and the pairwise peculiar velocity dispersion, $\sigma_{12},$ for all the CoDECS models. We find that for cDE models characterized by an exponential self-interaction potential, both a constant coupling and an exponentially growing coupling determine higher values of β and σ_{12} with respect to the ΛCDM case. On the contrary, Bouncing cDE models based on a SUGRA self-interaction potential predict a suppression of β and σ_{12} at $z\sim0.5-1,$ while at higher redshifts the differences with respect to the ΛCDM model decrease.

We also analyzed the geometric distortions induced by the DE coupling, finding that these are always negligible with respect to dynamical ones for all the exponential potential models, while they might have a comparable effect as the latter for the Bouncing cDE scenario.

Overall, we found a strong degeneracy of the DE coupling phenomenology with the amplitude of linear density perturbations defined by σ_8 : the clustering, the bias function and the RSD in cDE scenarios can be well reproduced by a standard ΛCDM model after having rescaled the matter power spectrum to the σ_8 normalization of each cDE model, for scales larger than $\sim 5-10~h^{-1}\,\text{Mpc}$. However, we also find that the σ_8 degeneracy is broken at smaller scales. Our results therefore suggest that it is possible to put strong constraints on the coupling between DE and CDM exploiting the shape of redshift-space clustering anisotropies and comparing the clustering and bias functions at small and large scales.

To conclude, we performed an extended analysis of the impact of an interaction between DE and CDM on the clustering and redshift-space distortions properties of CDM haloes, using state-of-the-art N-body simulations for these cosmologies. Although the effect of the coupling is highly degenerate with σ_8 at large scales, at smaller scales the degeneracy is broken, offering the chance that the next generation of wide and high-precision measurements of the galaxy distribution in real- and redshift-space might be able to tightly constrain or possibly detect a new interaction in the dark sector.

ACKNOWLEDGMENTS

We warmly thank C. Carbone and E. Branchini for helpful discussions and suggestions. We acknowledge financial contributions from contracts ASI-INAF I/023/05/0, ASI-INAF I/088/06/0, ASI I/016/07/0 COFIS, ASI Euclid-DUNE I/064/08/0, ASI-Uni Bologna-Astronomy Dept. Euclid-NIS I/039/10/0, and PRIN MIUR Dark energy and cosmology with large galaxy surveys. MB is supported by the DFG Cluster of Excellence "Origin and Structure of the Universe" and by the TRR33 Transregio Collaborative Research Network on the "Dark Universe". MB also acknowledges the HPC-Europa2 visiting programme for financial support

during his visits to the Astronomy Department in Bologna.

REFERENCES

Alcock C., Paczynski B., 1979, Nature, 281, 358
Allen S. W., Schmidt R. W., Ebeling H., Fabian A. C., van Speybroeck L., 2004, Mon. Not. R. Astron. Soc., 353, 457
Amendola L., 2000, Phys. Rev. D, 62, 043511
Amendola L., 2004, Phys. Rev. D, 69, 103524

Amendola L., Baldi M., Wetterich C., 2008, Phys. Rev. D, 78, 023015

Astier P., et al., 2006, Astron. Astrophys., 447, 31

Astier P., et al., 2006, Astron. Astrophys., 447, 31

Baldi M., 2011a, Mon. Not. Roy. Astron. Soc., 414, 116

Baldi M., 2011b, Mon. Not. Roy. Astron. Soc. submitted [arXiv:1107.5049]

Baldi M., 2011c, arXiv:1109.5695

Baldi M., 2011d, Mon. Not. Roy. Astron. Soc., 411, 1077

Baldi M., Pettorino V., 2011, Mon. Not. Roy. Astron. Soc., 412, L1

Baldi M., Pettorino V., Robbers G., Springel V., 2010, Mon. Not. Roy. Astron. Soc., 403, 1684

Baugh C. M., Gaztanaga E., Efstathiou G., 1995, Mon. Not. R. Astron. Soc., 274, 1049

Binney J. J., Evans N. W., 2001, Mon. Not. R. Astron. Soc., 327, L27

Brax P. H., Martin J., 1999, Physics Letters B, 468, 40

Cabré A., Gaztañaga E., 2009a, Mon. Not. R. Astron. Soc., 393, 1183

Cabré A., Gaztañaga E., 2009b, Mon. Not. R. Astron. Soc., 396, 1119

Carnero A., Sanchez E., Crocce M., Cabre A., Gaztanaga E., 2011, ArXiv e-prints

Clemson T., Koyama K., Zhao G.-B., Maartens R., Valiviita J., 2011, arXiv:1109.6234

Crocce M., Gaztanaga E., Cabre A., Carnero A., Sanchez E., 2011, ArXiv e-prints

Davis M., Efstathiou G., Frenk C. S., White S. D. M., 1985, Astrophys. J., 292, 371

Guzzo L., et al., 2008, Nature, 451, 541

Hamilton A. J. S., 1992, Astrophys. J. Lett., 385, L5

Hawkins E., et al., 2003, Mon. Not. R. Astron. Soc., 346, 78

Honorez L. L., Reid B. A., Mena O., Verde L., Jimenez R., 2010, JCAP, 1009, 029

Jackson J. C., 1972, Mon. Not. R. Astron. Soc., 156, 1P

Jee M. J., Rosati P., Ford H. C., Dawson K. S., Lidman C., Perlmutter S., Demarco R., Strazzullo V., Mullis C., Böhringer H., Fassbender R., 2009, Astrophys. J., 704, 672

Komatsu E., et al., 2009, Astrophys. J. Suppl., 180, 330

Komatsu E., et al., 2011, Astrophys. J. Suppl., 192, 18

Kowalski M., et al., 2008, Astrophys. J., 686, 749

Koyama K., Maartens R., Song Y.-S., 2009, JCAP, 0910, 017

Landy S. D., Szalay A. S., 1993, Astrophys. J., 412, 64

LaRoque S. J., Bonamente M., Carlstrom J. E., Joy M. K., Nagai D., Reese E. D., Dawson K. S., 2006, Astrophys. J., 652, 917 Laureijs R., 2009, ArXiv e-prints

Lee J., Baldi M., 2011, arXiv:1110.0015

Lewis A., Bridle S., 2002, Phys. Rev. D, 66, 103511

Linder E. V., 2008, Astroparticle Physics, 29, 336

Lucchin F., Matarrese S., 1985, Phys. Rev. D, 32, 1316

Marulli F., Bonoli S., Branchini E., Gilli R., Moscardini L., Springel V., 2009, Mon. Not. R. Astron. Soc., 396, 1404

Marulli F., Carbone C., Viel M., Moscardini L., Cimatti A., 2011, Mon. Not. R. Astron. Soc., 418, 346

Matsubara T., 2004, Astrophys. J., 615, 573

Mo H. J., Jing Y. P., Boerner G., 1992, Astrophys. J., 392, 452

Mortonson M. J., Hu W., Huterer D., 2011, Phys. Rev. D, 83, 023015

Newman A. B., Treu T., Ellis R. S., Sand D. J., Richard J., Marshall P. J., Capak P., Miyazaki S., 2009, Astrophys. J., 706, 1078

- Okumura T., Matsubara T., Eisenstein D. J., Kayo I., Hikage C., Szalay A. S., Schneider D. P., 2008, Astrophys. J., 676, 889
- Peacock J. A., et al., 2001, Nature, 410, 169
- Percival W. J., et al., 2001, Mon. Not. R. Astron. Soc., 327, 1297
- Percival W. J., et al., 2004, Mon. Not. R. Astron. Soc., 353, 1201
- Perlmutter S., et al., 1999, Astrophys. J., 517, 565
- Pettorino V., Baccigalupi C., 2008, Phys. Rev. D, 77, 103003
- Refregier A., et al., 2010, arXiv:1001.0061
- Riess A. G., et al., 1998, Astron. J., 116, 1009
- Rosati P., et al., 2009, Astron. Astrophys., 508, 583
- Schlegel D. J., et al., 2009, ArXiv e-prints
- Schmidt B. P., et al., 1998, Astrophys.J., 507, 46
- Scoccimarro R., 2004, Phys. Rev. D, 70, 083007
- Sherwin B. D., et al., 2011, ArXiv e-prints
- Sheth R. K., Mo H. J., Tormen G., 2001, Mon. Not. R. Astron. Soc., 323, 1
- Simon J. D., Bolatto A. D., Leroy A., Blitz L., 2003, Astrophys. J., 596, 957
- Smith R. E., Peacock J. A., Jenkins A., White S. D. M., FrenkC. S., Pearce F. R., Thomas P. A., Efstathiou G., CouchmanH. M. P., 2003, Mon. Not. R. Astron. Soc., 341, 1311
- Spergel D. N., et al., 2003, Astrophys. J. Suppl., 148, 175
- Springel V., 2005, Mon. Not. R. Astron. Soc., 364, 1105
- Springel V., Yoshida N., White S. D. M., 2001, New Astronomy, 6, 79
- Tegmark M., et al., 2004, Astrophys. J., 606, 702
- Tegmark M., et al., 2006, Phys. Rev. D, 74, 123507
- Tinker J. L., Robertson B. E., Kravtsov A. V., Klypin A., Warren M. S., Yepes G., Gottlöber S., 2010, Astrophys. J., 724, 878
- Ursino E., Branchini E., Galeazzi M., Marulli F., Moscardini L., Piro L., Roncarelli M., Takei Y., 2011, Mon. Not. R. Astron. Soc., 414, 2970
- Vikhlinin A., Kravtsov A., Forman W., Jones C., Markevitch M., Murray S. S., Van Speybroeck L., 2006, Astrophys. J., 640, 691
- Waizmann J.-C., Ettori S., Moscardini L., 2011, Mon. Not. R. Astron. Soc., pp 1415—+
- Wetterich C., 1988, Nuclear Physics B, 302, 668
- Wetterich C., 1995, Astron. Astrophys., 301, 321
- White S. D. M., 1994, ArXiv Astrophysics e-prints
- Zehavi I., Eisenstein D. J., Nichol R. C., Blanton M. R., Hogg D. W., Brinkmann J., Loveday J., Meiksin A., Schneider D. P., Tegmark M., 2005, Astrophys. J., 621, 22